Using Deuterium NMR Line Shapes To Analyze Lyotropic Liquid Crystalline Phase Transitions

John C. Blackburn and Peter K. Kilpatrick*

Department of Chemical Engineering, North Carolina State University, Raleigh, North Carolina 27695-7905

Received January 27, 1992. In Final Form: March 16, 1992

Deuterium quadrupole NMR line shapes were simulated to match experimental spectra of liquid crystalline phases observed in the cesium and sodium *n*-tetradecanoate–D_2O systems. The line shapes of single-phase samples with both uniaxial and biaxial symmetry were accurately simulated. Line shape simulations were matched to experimental spectra by minimizing the sum of squared residuals on the basis of local intensity maxima and minima. The line shape parameters optimized were the quadrupole splitting $\Delta\nu_Q$, the spin–spin relaxation time T_2, and, in the case of biaxial spectra, the aggregate asymmetry parameter η_D. The line shapes of multiple-phase samples were also accurately simulated by optimizing the relative amounts of each phase. The method can be used to accurately determine tie-line and tie-triangle end points in multiple-phase liquid crystal samples. Among the illustrative liquid crystalline transitions provided are hexagonal to ribbon phase, ribbon to lamellar phase, and ribbon to viscous isotropic phase.

Introduction

Surfactant molecules are amphiphilic, that is, possessing both hydrophilic and lipophilic moieties. Because of this dual character, surfactants aggregate when introduced into a solvent at sufficient concentration. At high concentration (>10 mol %), surfactants form liquid crystalline phases, consisting of structures dependent upon composition, temperature, surfactant, and solvent. Surfactants are used in many technological applications, including cleaning, food processing,[1] and protein separation.[2] The accurate determination of surfactant phase behavior is an essential step toward better understanding of physical properties, leading to development and improvement of surfactant-based applications.

The liquid crystalline phase behavior of anionic surfactant–water systems has been studied using several different experimental techniques.[3-40] X-ray diffraction has been used[3-10] to confirm the structure of the hexagonal and lamellar phases, and to quantify the dimensions of the unit cell in lyotropic surfactant liquid crystals. In addition, the method has been used to support proposed structures for liquid crystalline phases intermediate in composition between the hexagonal and lamellar phases. This technique is best suited for determining the structure of a single-phase sample. Data are collected in an X-ray experiment as a film exposure of the diffraction pattern or as an angle-dependent scattering intensity plot. A single crystalline sample would result in exposed spots corresponding to the lattice structure in Fourier space of the crystal. Most liquid crystal samples contain microdomains, resulting in an exposure which is a set of rings separated by characteristic spacings. Powder samples sometimes suffer from poor resolution of diffraction lines which can lead to difficulty in definitive identification of structure. The addition of a second or third phase to the sample further complicates the analysis.

* To whom correspondence should be addressed.

(1) Gillberg, G. Practical uses of microemulsions. In *Emulsions and emulsion technology*; Lissant, K. J., Ed.; Marcel Dekker: New York, 1984; Part 3.
(2) Powers, J. D.; Kilpatrick, P. K.; Carbonell, R. G. *Biotechnol. Bioeng.* **1990**, *33*, 506–519.
(3) Luzzati, V.; Mustacchi, H.; Skoulios, A. *Nature* **1957**, *180*, 600–601.
(4) Luzzati, V.; Mustacchi, H.; Skoulios, A. *Discuss. Faraday Soc.* **1958**, *25*, 43–50.
(5) Luzzati, V.; Mustacchi, H.; Skoulios, A.; Husson, F. *Acta Crystallogr.* **1960**, *13*, 660–667.
(6) Skoulios, A. *Adv. Colloid Interface Sci.* **1967**, *1*, 79–110.
(7) Leigh, I. D.; McDonald, M. P.; Wood, R. M.; Tiddy, G. J. T.; Trevethan, M. A. *J. Chem. Soc., Faraday Trans. 1*, **1981**, *77*, 2867–2876.
(8) Kekicheff, P.; Cabane, B. *J. Phys. (Paris)* **1987**, *48*, 1571–1583.
(9) Kekicheff, P.; Grabielle-Mondelmont, C.; Ollivon, M. *J. Colloid Interface Sci.* **1989**, *131*, 112–131.
(10) Kekicheff, P. *J. Colloid Interface Sci.* **1989**, *131*, 132–152.
(11) McBain, J. W.; Vold, R. D.; Vold, M. J. *J. Phys. Chem.* **1938**, *60*, 1866–1869.
(12) McBain, J. W.; Johnston, S. A. *J. Am. Chem. Soc.* **1941**, *63*, 875.
(13) Rosevear, F. B. *J. Am. Oil Chem. Soc.* **1954**, *31*, 628.
(14) Rosevear, F. B. *J. Am. Oil Chem. Soc.* **1968**, *19*, 581–594.
(15) Rendall, K.; Tiddy, G. J. T.; Trevethan, M. A. *J. Chem. Soc., Faraday Trans. 1* **1983**, *79*, 637–649.
(16) Blackburn, J. C.; Kilpatrick, P. K. *J. Colloid Interface Sci.* **1992**, *149*, 450–471.
(17) Demus, D.; Richter, L. *Textures of Liquid Crystals*; Weinhem: New York, 1978.
(18) Madelmont, C.; Perron, R. *Colloid Polym. Sci.* **1976**, *254*, 581–595.
(19) Kaneshina, S.; Yamanaka, M. *J. Colloid Interface Sci.* **1989**, *131*, 493–497.
(20) Casillas, N.; Puig, J. E.; Olayo, R.; Hart, T. J.; Franses, E. I. *Langmuir* **1989**, *5*, 384–389.
(21) Johansson, A.; Drakenberg, T. *Mol. Cryst. Liq. Cryst.* **1971**, *14*, 23–48.
(22) Johansson, A.; Lindman, B. In *Liquid Crystals and Plastic Crystals*; Gray, Winsor, Eds.; Wiley: New York, 1974; p 192.
(23) Wennerstrom, H.; Lindblom, G.; Lindman, B. *Chem. Scr.* **1974**, *6*, 97–103.
(24) Persson, N. O.; Fontell, K.; Lindman, B.; Tiddy, G. J. T. *J. Colloid Interface Sci.* **1975**, *53* (3), 461–466.
(25) Seelig, J. *Q. Rev. Biophys.* **1977**, *10*, 353–418.
(26) Forrest, B. J.; Reeves, L. W. *Chem. Rev.* **1981**, *81*, 1–14.
(27) Chidichimo, G.; Vaz, N. A. P.; Yaniv, Z.; Doane, J. W. *Phys. Rev. Lett.* **1982**, *49*, 1950–1954.
(28) Khan, A.; Fontell, K.; Lindblom, G.; Lindman, B. *J. Phys. Chem.* **1982**, *86*, 4266–4271.
(29) Davis, J. H. *Biochim. Biophys. Acta* **1983**, *737*, 117–171.
(30) Khan, A.; Fontell, K.; Lindman, B.; *J. Colloid Interface Sci.* **1984**, *101*, (1), 193–200.
(31) Chidichimo, G.; Golemme, A.; Doane, J. W.; Westerman, P. W. *J. Chem. Phys.* **1985**, *82*, 536–540.
(32) Chidichimo, G.; Golemme, A.; Doane, J. W. *J. Chem. Phys.* **1985**, *82*, 4369–4375.
(33) Doane, J. W. Determination of Biaxial Structures in Lyotropic Materials by Deuterium NMR. *NATO ASI Ser., Ser. C* **1985**, *151* 413–419.
(34) Lindman, B. *J. Colloid Interface Sci.* **1986**, 499–510.
(35) Lindman, B.; Soderman, O.; Wennerstrom, H. *Ann. Chim. (Rome)* **1987**, *77*, 1–48.
(36) Pope, J. M.; Doane, J. W. *J. Chem. Phys.* **1987**, *87*, 3201–3206.
(37) Kilpatrick, P. K.; Bogard, M. A. *Langmuir* **1988**, *4*, 790–796.
(38) Quist, P.; Halle, B. *Mol. Phys.* **1988**, *65*, 547.
(39) Khan, A. NMR of liquid crystals and micellar solutions. *Nucl. Magn. Reson.* **1989**, *18*, 408–448.
(40) Kilpatrick, P. K.; Blackburn, J. C.; Walter, T. A. *Langmuir*, submitted for publication.

0743-7463/92/2408-1679$03.00/0

Polarizing microscopy is one of the most widely used techniques[11-17] for phase identification. Information has been published identifying observed microscope textures and the corresponding phase structures. The characteristic texture observed using polarized light results from the defect structure of the sample.[17] Ideally, the defect pattern is phase-specific, with a particular microscope texture reflecting a given phase. When a second or third phase exists in a sample, the phases must be segregated to prevent inconclusive or misleading results. Microscopic textures of multiple-phase samples do not typically enable the determination of the relative amounts of each phase.

Differential scanning calorimetry (DSC) has also been used[9,18-20] to study phase transitions in liquid crystal systems. By monitoring the heat input to a sample while scanning in temperature, a phase transition is detected as the enthalpy of the phase transition, typically large compared to the sensible heat of the sample. DSC is useful for the characterization of the temperature and the enthalpy of phase transitions, but does not provide any information regarding the identity of a specific phase. Because it is a dynamic technique, questions arise regarding the deviation from equilibrium which occurs during the experiment.

Quadrupole nuclear magnetic resonance (NMR) spectroscopy is well-suited to the study of liquid crystalline phase behavior, and has been used widely to identify both single- and multiple-phase samples.[7,10,15,16,21-40] Deuterium (D) has a nuclear spin quantum number (I) of 1, possesses a quadrupole moment (eQ), and can be isotopically substituted as a probe in either the hydrogenated surfactant chains or water. A single anisotropic liquid crystalline phase exhibits a characteristic NMR line shape which depends on the anisotropy, geometry, and domain size of the liquid crystalline aggregates, and on the motion of the D_2O molecules. The spectrum of a multiple-phase sample is composed of the sum of the individual phase spectra, each of which is typically distinguishable.

The purpose of this paper is to present a technique for extracting quantitative phase composition data from experimental deuterium NMR spectra. We have used previously reported techniques[25,29] to calculate NMR line shapes which match experimental data for uniaxial and biaxial liquid crystalline phases in the CsTD–D_2O and the NaTD–D_2O systems. Multiple-phase spectra were calculated as the sum of single-phase theoretical spectra, again to match experimental spectra. In all cases the fitting was optimized using a least-squares minimization.

The amount of D_2O in a given phase is proportional to the integral of that portion of the spectrum, which can be resolved in a sample containing ca. 5% or more of a phase. Even when there are small domains of each phase or when one phase is dispersed in another, the composite spectrum contains representative information about each phase. Using the amounts of each phase in a sample and the composition of the sample, the compositional extent of the two-phase region has been calculated. This technique provides a good measure of the extent of the two-phase region using a small number of samples (equal to the number of coexisting phases).

The types of phase transitions observed in these surfactant–water systems and studied using line shape analysis can be categorized according to the symmetry of the aggregates: (i) uniaxial to biaxial (second order), (ii) biaxial to uniaxial (first order), (iii) biaxial to isotropic, (iv) uniaxial to isotropic, and (v) uniaxial to uniaxial. The temperature–composition phase diagrams for the cesium n-tetradecanoate (CsTD)–D_2O[16] and sodium n-tetradecanoate (NaTD)–D_2O[40] systems are presented in Figure 1. The single-phase regions are white, with two-phase regions indicated by hatching. The horizontal bars indicate the temperature and composition locations of the phase transitions discussed in this paper.

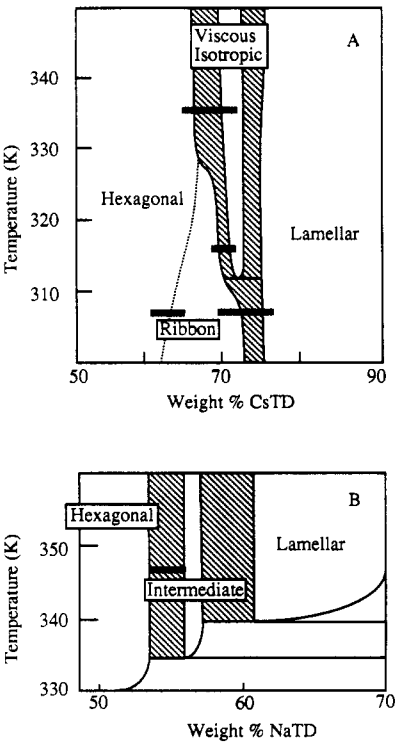

Figure 1. (A) Phase diagram of the cesium n-tetradecanoate (CsTD)–water (D_2O) system from 300 to 350 K denoting regions of liquid crystalline phase coexistence.[14] The phase behavior was determined using deuterium NMR in conjunction with polarizing microscopy. Single-phase regions are indicated in white with intervening two-phase regions hatched. The horizontal bars denote the temperature and compositional locations of the experimental spectra presented throughout the paper. (B) Phase diagram of the sodium n-tetradecanoate (NaTD)–D_2O system from 330 to 360 K, with hatching denoting regions of liquid crystalline phase coexistence.[40]

Theory of Quadrupole NMR

Quadrupolar nuclei (nuclear spin quantum number $I \geq 1$) interact with electric field gradients such as those existing on the surface of ionic surfactant aggregates. Quadrupolar nuclei in an anisotropic environment experience an ordering measured by the residual quadrupolar coupling constant $\langle\chi\rangle$. Vibrational and rotational motion are rapid compared to the relaxation rate of the nucleus and reduce the observed value from the static coupling value ($\chi = 220$ kHz)[41] by averaging the orientation of the quadrupolar nucleus over the time period of the relaxation:

$$\langle\chi\rangle = (e^2Qq/2h)\langle 3\cos^2\theta_{DM} - 1 + \eta_M \sin^2\theta_{DM}\cos 2\phi_M\rangle_{DM} \quad (1)$$

The quadrupole moment of the nucleus (eQ), the electric field gradient (eq), and the orientation of the z-axis of the molecular reference frame (θ_{DM}, ϕ_M) with respect to the liquid crystalline aggregate director determine the magnitude of the coupling constant. The coupling is averaged

(41) Halle, B.; Wennerstrom, H.; *J. Chem. Phys.* **1981**, *75*, 1928–1943.
(42) Abragam, A. *Principles of Nuclear Magnetism*; Oxford University Press: Oxford, 1961.
(43) Poole, C. P.; Farach, H. A. *Theory of Magnetic Resonance*, 2nd ed.; Wiley: New York, 1987.
(44) Cohen, M.; Reif, E. *Solid State Phys.* **1957**, *5*, 321–438.

over the time for quadrupolar relaxation (T_2) as indicated by $\langle ... \rangle_{DM}$. The asymmetry parameter (η_M) is a measure of the variation in electric field gradients ($\mathbf{V}_{ii}$) at the nucleus in a coordinate frame oriented in the D_2O molecule:

$$\eta = (V_{xx} - V_{yy})/V_{zz} \quad (2)$$

$\mathbf{V}_{ii}$ is a traceless tensor consisting of the diagonalized components of the electric field gradient tensor. The orientation of the coordinate frame is chosen such that $|V_{zz}| \geq |V_{yy}| \geq |V_{xx}|$.[25,29]

The quadrupole splitting is a measure of the anisotropy and orientation of the aggregate director axis which undergoes motion slow compared to the nuclear relaxation. For a domain of given orientation, the quadrupole splitting is determined by eq 3.[41] Here θ_{LD} and ϕ_D describe the

$$\Delta\nu_Q = [3\langle\chi\rangle/4I(2I-1)][3\cos^2\theta_{LD} - 1 + \eta_D \sin^2\theta_{LD}\cos 2\phi_D] \quad (3)$$

orientation of the aggregate director with respect to the externally applied magnetic field (H_0). The asymmetry parameter (η_D) is defined in the aggregate director frame and describes the variation of the electric field gradient on the surface of the surfactant aggregate.

Equation 3 describes the quadrupole splitting for a given domain of liquid crystal directors with the same orientation with respect to H_0. A sample consisting of a random distribution of uniaxial aggregates produces a characteristic Pake[45] or powder pattern spectrum:

$$F(\nu) = [1 \pm 8\nu/3\langle\chi\rangle]^{-1/2}/[3^{3/2}\langle\chi\rangle] \quad (4)$$

Equation 4 is the sum of two contributions for different ranges of ν. The line shape is the sum of the two curves as the "negative" contribution for $-3\langle\chi\rangle/4 < \nu < 3\langle\chi\rangle/8$ is added to the "positive" contribution for $-3\langle\chi\rangle/8 < \nu < 3\langle\chi\rangle/4$. There are singularities at $\nu = \pm 3\langle\chi\rangle/8$, and this separation ($3\langle\chi\rangle/4$) is the quadrupole splitting.

When $\eta_D \neq 0$, two angular integrations must be performed to evaluate the line shape function.[46] This transformation results in a deuterium line shape for biaxial aggregates of

$$F(\nu) = (4/\pi 3\langle\chi\rangle\eta_D)\int_0^1 d\gamma/[(1+\gamma)(1-\gamma)(3/\eta_D - \gamma) \times (4\nu/3\langle\chi\rangle\eta_D + 1/\eta_D - \gamma)]^{1/2} \quad (5)$$

Equation 5 yields half of the theoretical line shape; superimposing $F(\nu)$ and $F(-\nu)$ results in the full line shape. Equation 5 is an elliptic integral of the second kind, with $\gamma = \cos 2\phi$. Equations 4 and 5 represent the unbroadened line shape functions for polycrystalline uniaxial and biaxial quadrupole spectra of a nucleus with spin quantum number $I = 1$.

Equations 4 and 5 yield line shapes with singularities which are not observed experimentally. Experimental spectra are broadened by quadrupolar relaxations due to the motion of D_2O molecules. To simulate these experimental effects, theoretical spectra can be broadened by convoluting the $F(\nu)$ function with a Lorentzian distribution:[47]

$$G(\nu) = \int_{-\infty}^{\infty} F(\nu')(1/1 + [(2\pi/a)(\nu - \nu')]^2)\, d\nu' \quad (6)$$

The convolution is equivalent to the sum of Lorentzian line shapes located at every frequency weighted by the intensity of the given frequency. The broadening calculation transforms each doublet with zero line width to a doublet of Lorentzian line shapes, each with a half-height width of a in dimensionless terms. When the broadening is referenced to the quadrupole splitting, it can be expressed in hertz, which is the reciprocal of the spin–spin relaxation time T_2.

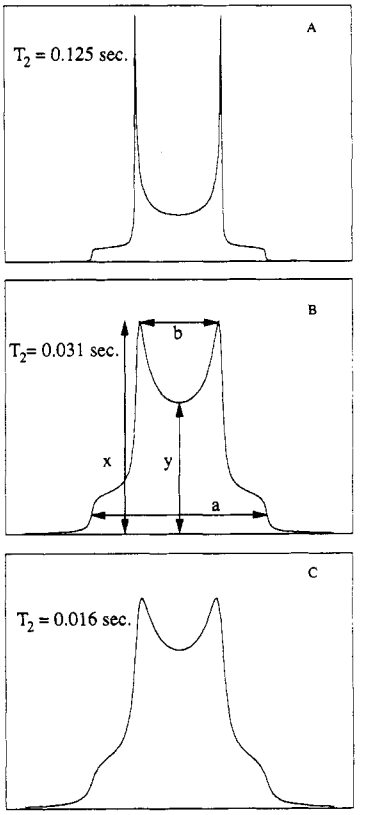

Figure 2. Theoretical spectra of a quadrupolar nucleus (nuclear spin $I = 1$) in an anisotropic, uniaxial environment demonstrating the effect of changing the spin relaxation time (T_2). The values used are (A) 0.125 s, (B) 0.031 s, and (C) 0.016 s. The horizontal measurements used for fitting uniaxial deuterium NMR spectrum are a, width at inflection point of shoulders, and b, peak separation. The vertical measurements are x, maximum height of spectrum, or mean if two peaks differ in height, and y, height of spectrum at central frequency.

Figure 2 is a set of theoretical uniaxial line shapes for a range of relaxation times for spectra with the same quadrupole splitting. These line shapes were calculated using eqs 4 and 6 with a quadrupole splitting of 1000 Hz and T_2 values of 0.13, 0.031, and 0.016 s, respectively. There is a pronounced decrease in the separation of the maxima in the spectra, as the relaxation time is decreased. The decrease from the unbroadened quadrupole splitting is ca. 8% for T_2 = 0.13 s, and 13% for T_2 = 0.016 s. By determining the amount of line broadening, uniaxial powder pattern line shapes can be fit fairly easily.

Figure 3 shows the effect of varying the asymmetry parameter while the broadening remains constant (T_2 = 0.063 s): (A) η_D = 0.2, (B) η_D = 0.4, and (C) η_D = 0.7. For a constant value of the quadrupole splitting, as shown by the same width of the base of the spectrum, the peak maxima separation decreases as η_D increases. The quadrupole splitting and the asymmetry parameter can be measured directly from the spectrum; the width of the base is twice the quadrupole splitting ($2\Delta\nu_Q$), and the peak separation is $(1 - \eta_D)\Delta\nu_Q$. When the spectrum is well

(45) Pake, G. E. *J. Chem. Phys.* **1948**, *16*, 327–351.
(46) Haeberlen, U. *High Resolution NMR in Solids: Selective Averaging*; Academic Press: New York, 1976.
(47) Siderer, Y.; Luz, Z. *J. Magn. Reson.* **1980**, *37*, 449–463.

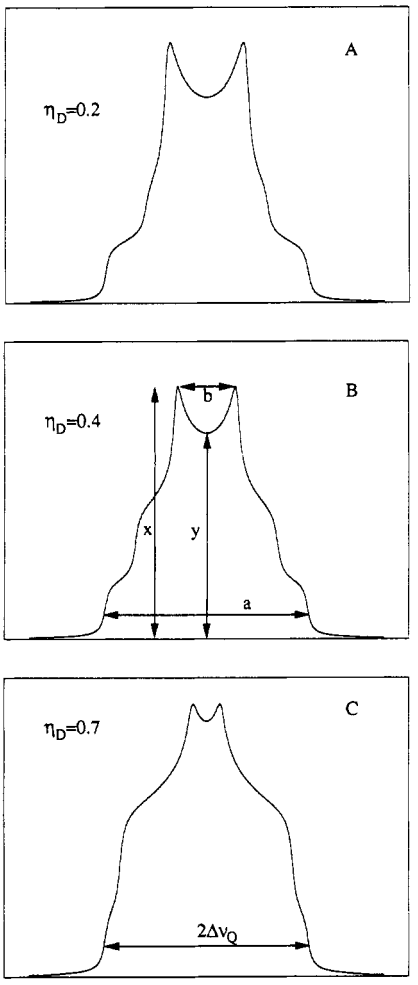

Figure 3. Theoretical line shapes for a spin $I = 1$ nucleus for a range of asymmetry parameters (η_D), simulating the trend of NMR line shapes observed in the hexagonal to ribbon phase transition: (A) $\eta_D = 0.2$, (B) $\eta_D = 0.4$, and (C) $\eta_D = 0.7$. A T_2 value of 0.031 s was used to calculate all three line shapes. The characteristic horizontal measurements used for fitting biaxial deuterium NMR spectra are a, width at inflection point of shoulders, and b, peak separation (zero if only a single maximum). The vertical measurements are x, maximum height of spectrum, or mean if two peaks differ in height, and y, height of spectrum at central frequency.

defined, as shown in the theoretical line shapes, a second inflection pair is apparent with a separation equal to $(1 + \eta_D)\Delta\nu_Q$.

Experimental Section

Materials. Sodium *n*-tetradecanoate (NaTD) was purchased from Nu Chek, Prep, Inc. (Elysian, MN), and used without further purification. Cesium *n*-tetradecanoate (CsTD) was synthesized by reacting equimolar amounts of cesium hydroxide (99.98%, Carus Chemical Co., LaSalle, IL) and *n*-tetradecanoic acid (99.5%, Gold Label, Aldrich). Each reagent was dissolved in HPLC grade methanol (Fisher), which was removed from the reaction product by rotary evaporation. The purified surfactant was dried at 5 Torr and 40 °C and stored in a desiccator over calcium sulfate. The purity of the surfactant was determined to be >98% by elemental analysis. The melting temperature of the dry surfactant was determined by DSC to be 290 °C, in agreement with the literature.[48] Deuterium oxide (99.8% D, Wilmad Glass) was used without further purification. Hydrogenated water used for ampule samples was doubly distilled.

Methods. Sample Preparation. Surfactant–water samples were made in both 5-mm NMR tubes (Wilmad Glass), using deuterium oxide in place of water, and 5-mL glass ampules for visual observations. The surfactant was weighed into the sample container, the corresponding amount of water or deuterium oxide was added, and the container was flame-sealed to maintain compositional integrity. The composition of the samples, accurate to ±0.1 wt %, was calculated and reported on a deuterium-free basis, that is, the composition corresponding to the use of hydrogenated water rather than deuterium oxide. The samples equilibrated in a circulating air bath maintained at 67 °C to within 0.5 °C during normal operation and to within 1 °C when the chamber was being used for visual observations. The samples equilibrated for 1–13 months in the air bath or in a circulating water bath to investigate a range of temperatures. After samples had reached equilibrium at 67 °C, they were allowed to reequilibrate at a new temperature for at least 1 week before NMR experiments were performed. Samples were rerun 2–10 weeks later to guarantee that equilibrium had been reached.

NMR Spectroscopy. ^{2}H NMR spectra were obtained with an IBM CX-100 spectrometer, operating in the Fourier transform (FT) mode, equipped with an IBM VTU temperature controller. Spectra were taken at a resonance frequency of 15.371 MHz, with a typical spectral width of 5000–20000 Hz, 500–1000 transients, a pulse width of 12 μs ($\pi/2$), and an acquisition time of 0.1–0.3 s depending on the time constant of the free induction decay of the sample being analyzed.

Results and Discussion

Single-Phase Line Shape Fitting. The liquid crystalline phase behavior of surfactant (CsTD, NaTD)–water (D_2O) samples as determined using quadrupole NMR has been reported previously.[15,16,40] In this paper we use eqs 4–6 to calculate theoretical line shapes, which match experimental spectra. Uniaxial spectra are entirely determined by two parameters, the quadrupole splitting ($\Delta\nu_Q$) and the relaxation time (T_2). The quadrupole splitting can be approximated by the peak separation or by half the width of the spectral shoulders as shown in Figure 2A. T_2 cannot be extracted directly from the spectrum, and was determined using a least-squares minimization. Characteristic dimensions of the spectra were measured as shown in Figures 2B and 3B. The ratio of the two vertical measurements, the height of the peak maxima and the height of the central minimum, and the ratio of the two horizontal measurements, the peak separation and the width of the spectrum at the base, are used to compare the experimental and theoretical line shapes. By squaring the difference between the experimental and theoretical values of these ratios, theoretical line shapes were matched to experimental spectra by minimizing the residual:

$$\text{residual}_{\text{single-phase}} = \left(\frac{b_{\text{exptl}}}{a_{\text{exptl}}} - \frac{b_{\text{theor}}}{a_{\text{theor}}}\right)^2 + \left(\frac{y_{\text{exptl}}}{x_{\text{exptl}}} - \frac{y_{\text{theor}}}{x_{\text{theor}}}\right)^2 \quad (7)$$

Figure 4 contains experimental and optimized theoretical spectra of single liquid crystalline phase samples observed in the CsTD-D_2O system. The hexagonal phase (Figure 4a, 57.0 wt % CsTD, $\Delta\nu_Q$ = 555 Hz) is composed of surfactant rods packed on a hexagonal lattice, while the corresponding line shape (Figure 4b) is a broadened uniaxial spectrum. The variation of the residual (eq 7) as a function of the relaxation time (T_2) for a hexagonal phase spectrum is shown in Figure 5. It can be seen that the minimum in the residual, and thus the T_2 value to match the experimental spectrum, is 0.076 s.

An experimental spectrum of a ribbon phase sample is shown in Figure 4c; the ribbon phase has biaxial symmetry and is composed of deformed surfactant rods, where the cross-section is ellipsoidal rather than circular. Three parameters describe a biaxial spectrum: the quadrupole splitting ($\Delta\nu_Q$), the asymmetry parameter (η_D), and the

(48) Sanesi, M.; Franzosini, P. *Z. Naturforch.* 1984, *39a*, 362–365.

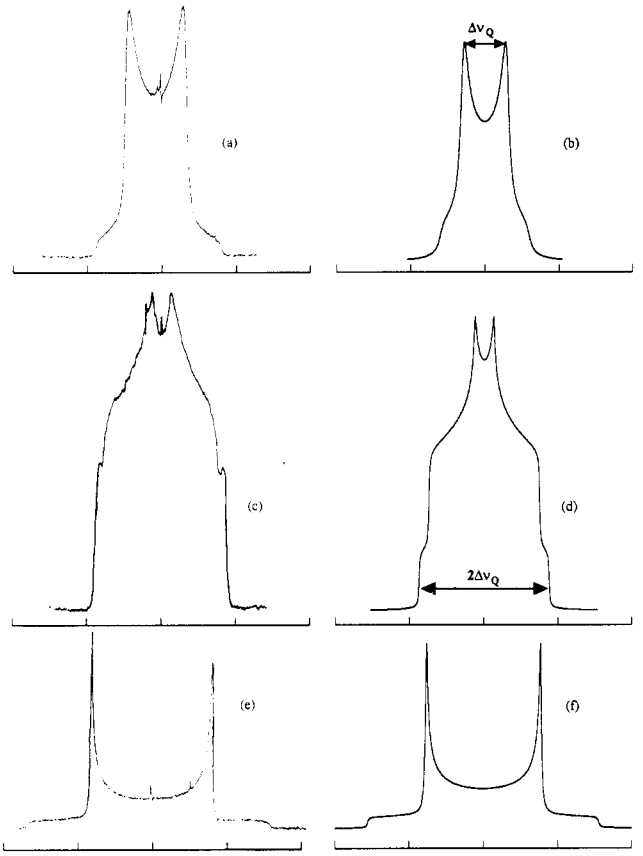

Figure 4. Experimental deuterium NMR spectra and theoretical line shapes of single-phase liquid crystalline samples in the CsTD–D_2O system taken at 308 K: (a) hexagonal phase spectrum (57.0 wt % CsTD, $\Delta\nu_Q$ = 555 Hz), (b) theoretical line shape ($\Delta\nu_Q$ = 555 Hz, T_2 = 0.07 s), (c) ribbon phase spectrum (66.5 wt % CsTD, $\Delta\nu_Q$ = 860 Hz, η_D = 0.6), (d) theoretical line shape ($\Delta\nu_Q$ = 860 Hz, T_2 = 0.1 s, η_D = 0.7), (e) lamellar phase spectrum (81.0 wt % CsTD, $\Delta\nu_Q$ = 1540 Hz), and (f) theoretical line shape ($\Delta\nu_Q$ = 1540 Hz, T_2 = 0.083 s). The tick marks are separated by 1000 Hz.

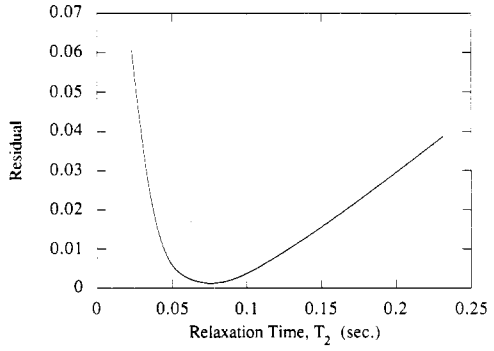

Figure 5. Variation of the residual calculated using eq 7 as a function of T_2, the spin relaxation time for the nuclei, to fit a hexagonal phase spectrum. The minimum of the cubic spline (0.076 s) was used to calculate the theoretical line shape in Figure 4b.

relaxation time (T_2). The quadrupole splitting ($\Delta\nu_Q$) is evaluated as half the measured width of the spectrum base (as shown in Figure 3). Optimized values of T_2 and η_D were evaluated using eq 7 to calculate the residuals. The residual again was calculated from the differences between experimental and theoretical values of the vertical and horizontal ratios. The η_D dependence and the T_2 dependence of the residual are shown in Figure 6. The optimized parameter values (η_D = 0.7, T_2 = 0.10 s) were used to calculate the theoretical ribbon (R)-phase line shape (Figure 4d), which shows significant deviation from a uniaxial spectrum.

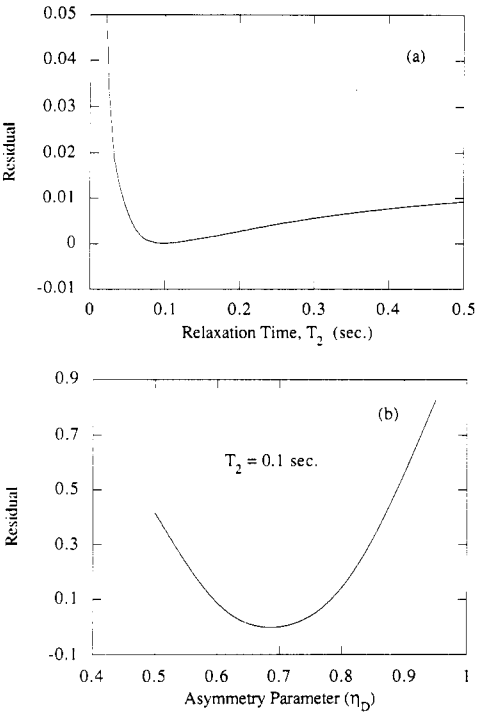

Figure 6. Variation of residual calculated using eq 7 as a function of T_2, the spin relaxation time, and η_D, the asymmetry parameter, to fit the experimental spectrum shown in Figure 4c. The minimum values of T_2 = 0.10 s and η_D = 0.68 were used to calculate the theoretical line shape in Figure 4d.

Table I. Summary of Phase Transitions, Phase Involved, and Order of the Phase Transitions

symmetry	phases[a]	surfactant	temp, K	order
uniaxial to biaxial	H_α to R	CsTD	308	second
biaxial to uniaxial	R to L_α	CsTD	308	first
biaxial to isotropic	R to VI	CsTD	315	first
uniaxial to isotropic	H_α to VI	CsTD	335	first
uniaxial to uniaxial	H_α to Int	NaTD	347	first

[a] The phases observed are labeled hexagonal (H_α), ribbon (R), lamellar (L_α), viscous isotropic (VI), and intermediate (Int).

An experimental spectrum of a lamellar phase sample is shown in Figure 4e; this phase is composed of surfactant bilayers separated by water layers. The matching line shape (Figure 4f) is a slightly broadened (T_2 = 0.083 s) uniaxial spectrum.

Phase Transitions. Single-phase liquid crystalline regions are separated by a phase transition, usually consisting of a two-phase region. Theoretical line shapes have been calculated to match experimental spectra of samples in the transition region. Five phase transitions are discussed in this paper and are presented in Table I, which collects the type of transition, the temperature and surfactant studied, and the order of the transition. Two liquid crystalline phases, not mentioned above, are listed in Table I. They are the viscous isotropic (VI) phase and the intermediate (Int) phase. The VI phase has cubic symmetry with a proposed structure consisting of interconnected rods on an *Ia3d* lattice[6,15,16] and is observed in the CsTD–D_2O system.[16] The Int phase is an anisotropic phase observed at compositions falling between those of the H_α and L_α phases in the NaTD–D_2O system.[15,18,37,40] The structure of the Int phase has not been determined definitively.

Hexagonal to Ribbon Phase Transition. The lowest concentration liquid crystalline phase observed in the CsTD–D_2O system is the hexagonal (H_α) phase. At 308 K an increase in surfactant concentration results in a

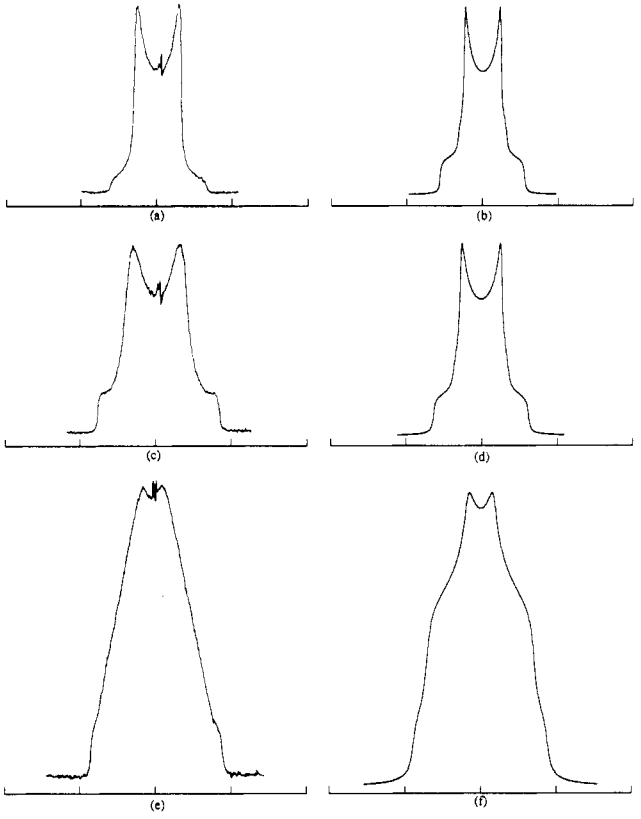

Figure 7. Experimental deuterium NMR spectra and theoretical line shapes for CsTD–D_2O samples spanning the hexagonal/ribbon phase second-order transition at 308 K: (a) hexagonal phase spectrum (57.0 wt % CsTD, $\Delta\nu_Q$ = 555 Hz), (b) theoretical line shape ($\Delta\nu_Q$ = 555 Hz, T_2 = 0.07 s), (c) ribbon phase spectrum (61.7 wt % CsTD, $\Delta\nu_Q$ = 810 Hz, η_D = 0.2), (d) theoretical line shape ($\Delta\nu_Q$ = 810 Hz, η_D = 0.15, T_2 = 0.04 s), (e) ribbon phase spectrum (64.0 wt % CsTD, $\Delta\nu_Q$ = 880 Hz, η_D = 0.7), and (f) theoretical line shape ($\Delta\nu_Q$ = 880 Hz, η_D = 0.6, T_2 = 0.024 s). The tick marks are separated by 1000 Hz.

second-order phase transition to the ribbon (R) phase.[16] Characteristic of a second-order phase transition, there is no coexistence region between the H_α and R phases. There is a smooth increase in the quadrupole splitting as the uniaxial hexagonal phase converts to the biaxial ribbon phase. Within the single hexagonal phase region, an increase in surfactant composition results in a decrease in the spacing between the surfactant rods which compose the aggregates. At the phase transition, rather than changing the separation between aggregates, the aggregates deform to an elliptic rather than circular cross-section. This results in a change in the surface asymmetry parameter from zero to a finite value ($0 < \eta_D < 1$).

A sequence of experimental spectra and matching theoretical line shapes in the hexagonal to ribbon phase transition region is shown in Figure 7. Both η_D and T_2 were optimized in generating the theoretical line shapes shown in Figure 7b,d,f. As is observed in all experimental spectra, there is a small isotropic D_2O peak falling in the middle of the spectra. This is a result of D_2O vapor in the space above the liquid crystal in the sample tube. When η_D has a value near 1, the resolution of the peak separation is obscured by a combination of line broadening and the small isotropic peak. In these experimental spectra, a separation of less than about 75 Hz could not be measured.

Line Shape Fitting of Two-Phase Spectra. A first-order phase transition is characterized by a region of phase coexistence separating two single-phase regions. Within the two-phase region, the composition of each phase does not vary with overall sample composition. The composition of each phase is determined by the location of the phase boundary, and the relative amount of each phase is set by the overall sample composition and the tie-lever rule. Consequently, the characteristic NMR spectra of the individual phases remain the same, while the intensity of each phase changes as the two-phase region is spanned. Using optimized single-phase spectra, the experimental spectra of two-phase samples were calculated as a weighted sum of the bounding single-phase line shapes. The residual for fitting two-phase spectra was calculated using characteristic measurements, dependent upon the shape of the composite spectrum, which are described in the following sections. In all cases, a least-squares difference of the relavent measurements between the theoretical line shape and the experimental spectra was used for optimization.

Ribbon to Lamellar Phase Transition. In the CsTD–D_2O system, at temperatures between 300 and 313 K, an increase in composition from 70 to 75 wt % CsTD results in a ribbon (R) phase to lamellar (L_α) phase transition. The R/L_α phase transition is between a biaxial phase and a uniaxial phase. The R phase in equilibrium with the L_α phase has an asymmetry parameter near unity, and the peak broadening is sufficient to eliminate two distinct peaks at the top of the spectrum. Spectra of R/L_α biphasic samples with only a small amount of L_α phase are distinctive because the sides of the spectrum are steeper than single R phase spectra. Figure 8a shows an experimental deuterium spectrum (73.6 wt % CsTD, 308 K) of a sample in the low composition portion of the two-phase region. As the surfactant composition increases, the amount of L_α phase apparent in the composite spectrum also increases. Figure 8c shows an experimental spectrum with a sufficient amount of L_α phase that the peaks of the powder pattern are discernible.

The measurement for optimization of the theoretical line shapes is the ratio of the height of the L_α phase powder pattern peaks to the height of the R phase central peak. In cases for which there is a minimum observed in the spectrum, such as in Figure 8c, the ratio of the minimum separation to the L_α phase quadrupole splitting is also used in the optimization. Optimized line shapes which match the experimental R/L_α phase spectra are presented in Figure 8b,d.

The quadrupole splitting value for each phase in these samples is measurable. In the experimental spectrum shown in Figure 8c (74.5 wt % CsTD), the outside portion of the spectrum enables the measurement of the ribbon phase quadrupole splitting, while the peaks give a measure of the L_α phase quadrupole splitting. The difference between these two values is identifiable by observing the curvature and inflection points in the vertical sides of the spectrum. It is here that the prominent feature of the spectrum changes from the ribbon portion to the lamellar phase portion. The inflection in the experimental spectrum can be seen in the theoretical spectrum (Figure 8d).

The phase diagrams presented in Figure 1 were generated using samples closely spaced in composition. Each sample was analyzed using deuterium NMR to detect single and two-phase spectra. This information was compiled to draw the phase boundaries. This method is tedious as many samples are needed to define the phase boundaries, with mistakes possible in distinguishing single and biphasic spectra near the boundary due to overlap of line shapes. By analyzing two-phase NMR spectra and determining the amount of each phase in a sample, phase

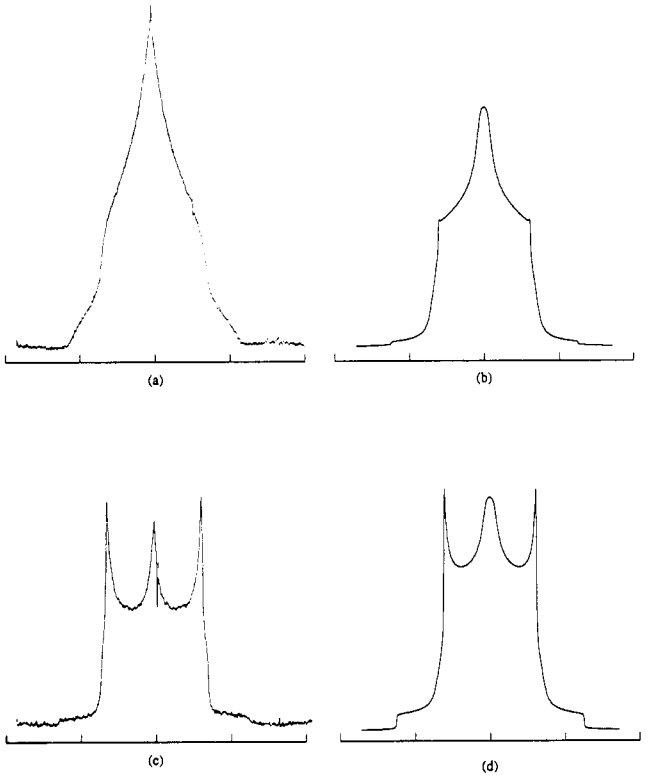

Figure 8. Experimental and theoretical deuterium NMR spectra of samples in the ribbon/lamellar phase transition region at 308 K: (a) two-phase spectrum (73.6 wt % CsTD; ribbon phase, $\Delta\nu_Q$ = 720 Hz, η_D = 0.8 ± 0.1; lamellar phase, $\Delta\nu_Q$ = 1270 Hz), (b) theoretical line shape (biaxial (80%), $\Delta\nu_Q$ = 720 Hz, η_D = 0.8, T_2 = 0.019 s; uniaxial (20%), $\Delta\nu_Q$ = 1270 Hz, T_2 = 0.05 s), (c) two-phase spectrum (74.5 wt % CsTD; ribbon phase, $\Delta\nu_Q$ = 720 Hz, η_D = 0.8 ± 0.1; lamellar phase, $\Delta\nu_Q$ = 1270 Hz), and (d) theoretical line shape (biaxial (40%), $\Delta\nu_Q$ = 720 Hz, η_D = 0.8, T_2 = 0.019 s; uniaxial (60%), $\Delta\nu_Q$ = 1270 Hz, T_2 = 0.05 s). The tick marks are separated by 1000 Hz. Measured characteristics used for the fitting of two-phase uniaxial + biaxial spectra are for horizontal measurements *a*, width at inflection point of shoulders, and *b*, minimum separation, and for Vertical measurements *x*, maximum height of spectrum, or mean if two peaks differ in height, *y*, height of spectrum at central frequency, and *z*, the height of the minimum.

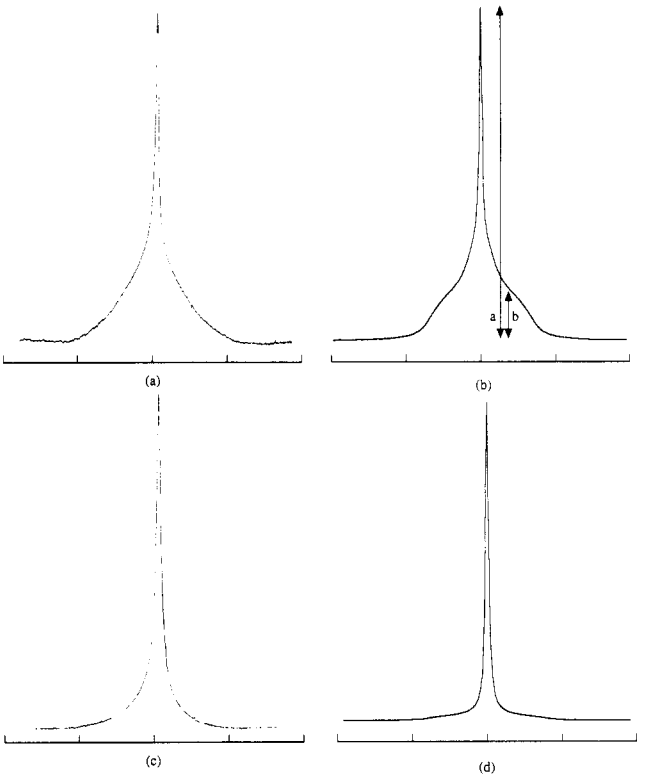

Figure 9. Experimental and theoretical deuterium NMR spectra of samples in the ribbon/VI phase transition region at 315 K: (a) two-phase spectrum (70.4 wt % CsTD; ribbon phase, $\Delta\nu_Q$ = 900 Hz), (b) theoretical line shape (biaxial (85%), $\Delta\nu_Q$ = 900 Hz, η_D = 0.6, T_2 = 0.014 s; isotropic (15%), T_2 = 0.067 s), (c) two-phase spectrum (71.1 wt % CsTD), and (d) theoretical line shape (biaxial (30%), $\Delta\nu_Q$ = 900 Hz, η_D = 0.6, T_2 = 0.014 s; isotropic (70%), T_2 = 0.067 s). The tick marks are separated by 1000 Hz. The residual is calculated from the ratio of the height of the spectrum at half-width and the total height.

boundaries can be determined using fewer samples and experiments.

By evaluating the amount of each phase in a two-phase sample, the location of the sample within the transitional region can be determined. Using two or more samples in the region, the end points of the transition can be calculated as well. Several samples within the transition region give a measure of accuracy of the phase boundary determination.

The R to L_α phase transition is first order as demonstrated by the existence of the two-phase region separating the single-phase regions. Two samples in the two-phase region were analyzed using line shape fitting (Figure 8). The calculated extent of the R/L_α multiple-phase region at 308 K is 73.2–75.1 wt % CsTD. Using the uncertainty of ±0.1 wt % CsTD for the individual samples, the uncertainty for the phase boundaries is ±0.2 wt % CsTD. These transition values obtained by line shape optimization compare favorably with those values of 72.8–74.8 wt % obtained by preparing many one-phase and two-phase samples to delineate the transition (Figure 1A).

Ribbon to Viscous Isotropic Phase Transition. At temperatures from 310 to 330 K, an increase in surfactant concentration from 70 to 75 wt % CsTD results in a ribbon (R) phase to viscous isotropic (VI) phase transition. Experimental and theoretical spectra of samples in the R/VI transition region, taken at 315 K, are shown in Figure 9. The most prominent characteristic of spectra containing VI phase is the sharp isotropic peak which is evident with more than ca. 5% VI phase in the sample. The existence of R phase in the sample is identifiable from the NMR spectrum as the width of the base of the spectrum increases dramatically from the single peak typical of a single VI phase sample.

The R/VI phase spectra were fit using the ratio of the isotropic peak height to the height of the spectrum at half of its width. The existence of a small amount of VI phase in the sample can be detected quite precisely as a distinctive change in the spectrum results. In the high concentration portion of the transition region, the amounts of R and VI phases cannot be calculated as precisely. The difficulty results from the shape of the two single-phase spectra. The integral of the respective spectral contributions is proportional to the amount of deuterium nuclei occupying each phase. Because of this, the single peak of the VI phase spectrum appears much more intense than the broad R-phase spectrum for a similar amount of each phase.

Using four data points, the calculated boundaries for the multiple phase region is 69.4–71.7 wt % CsTD, which compares very favorably with the values of 69.6–71.5 wt % obtained by the more time-consuming approach of preparing many single-phase and biphasic samples to delineate the transition (Figure 1A).

Hexagonal to Viscous Isotropic Phase Transition. At temperature above 330 K, the ribbon phase is not

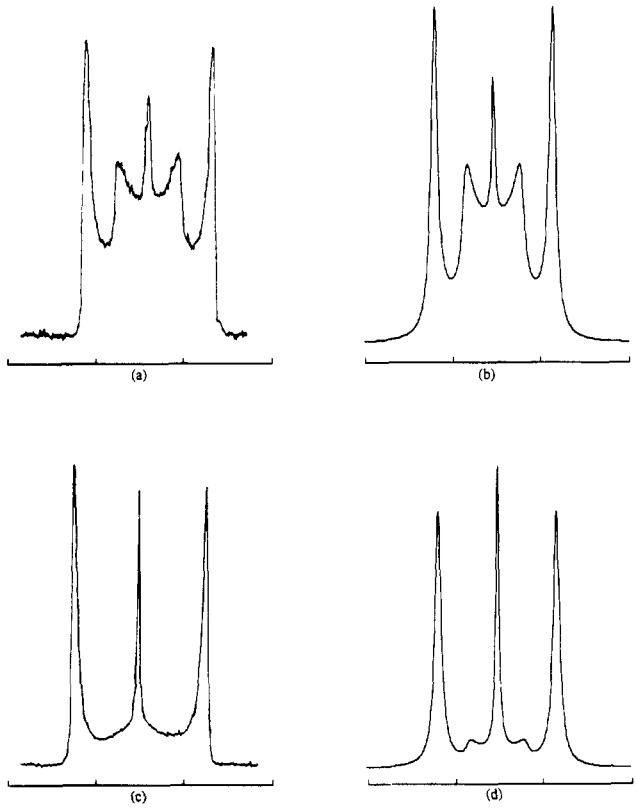

Figure 10. Experimental and theoretical deuterium NMR spectra of samples in the hexagonal/viscous isotropic phase transitional region at 335 K: (a) two-phase spectrum (65.8 wt % CsTD; hexagonal, $\Delta\nu_Q = 600$ Hz), (b) theoretical line shape (uniaxial (60%), $\Delta\nu_Q = 600$ Hz, $T_2 = 0.0095$ s; doublet (35%), $\Delta\nu_Q = 1200$ Hz, $T_2 = 0.04$ s; isotropic (4%), $T_2 = 0.067$ s), (c) two-phase spectrum (66.2 wt % CsTD; hexagonal, $\Delta\nu_Q = 600$ Hz), and (d) theoretical line shape (uniaxial (20%), $\Delta\nu_Q = 600$ Hz, $T_2 = 0.0095$ s; doublet (60%), $\Delta\nu_Q = 1200$ Hz, $T_2 = 0.04$ s; isotropic (20%), $T_2 = 0.067$ s). The tick marks are separated by 1000 Hz.

observed in the CsTD–D_2O system. At 335 K a phase transition from the H_α phase to the VI phase is observed. Experimental and optimized theoretical spectra of samples in the two-phase region are shown in Figure 10. The hexagonal portion of the spectra in this figure is typical of an oriented phase as the rod aggregates of the phase align with the walls of the NMR sample tube. As the directors of the liquid crystalline aggregates have a preferred orientation, the characteristic powder pattern appearance of the spectrum is lost. The oriented portion of the spectrum was simulated as a broadened doublet separated by twice the quadrupole splitting.

Using three two-phase spectral data points, the calculated extent of the H_α/VI phase transition at 335 K is 65.5–69.5 wt % CsTD. This compares with 66.0–69.5 wt % in Figure 1A.

Hexagonal to Intermediate Phase Transition. In the sodium *n*-tetradecanoate (NaTD)–D_2O system, the transitional phase which is observed compositionally between the hexagonal and lamellar phases is the intermediate (Int) phase.[40] The Int phase is anisotropic with an observed quadrupole splitting smaller than that observed in the hexagonal phase. At 347 K, the H_α/Int phase transition is observed. Experimental and optimized theoretical spectra of samples in the H_α/Int transition region are shown in Figure 11. The H_α and Int phases each have uniaxial symmetry as is reflected in the NMR spectra. The residual is calculated using the ratio of the height of the inner peaks and the height of the outer peaks,

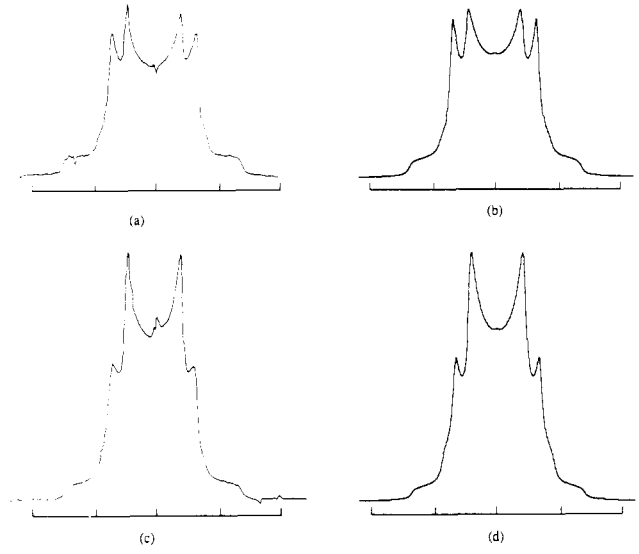

Figure 11. Experimental deuterium NMR spectra and theoretical line shapes for the hexagonal/intermediate phase transition in the NaTD–D_2O system at 347 K: (a) 53.8 wt % NaTD, $\Delta\nu_Q = 425$ Hz, 675 Hz, (b) theoretical line shape ($\Delta\nu_Q = 425$ Hz, $T_2 = 0.077$ s (40%); 675 Hz, $T_2 = 0.045$ s (60 %)), (c) 54.4 wt % NaTD, $\Delta\nu_Q = 425$ Hz, 675 Hz, and (d) theoretical line shape ($\Delta\nu_Q = 425$ Hz, $T_2 = 0.077$ s (65%); 675 Hz, $T_2 = 0.045$ s (35%)). The tick marks are separated by 1000 Hz. The horizontal measurements used for fitting uniaxial + uniaxial two-phase spectra are *a*, width of peak separation for larger quadrupole splitting, and *b*, width at minimum. The vertical measurements are *x*, maximum height of spectrum with the larger quadrupole splitting, or mean if two peaks differ in height, and *y*, maximum height of spectrum with the smaller quadrupole splitting.

and the ratio of the minimum between the two sets of peaks and the outer quadrupole splitting peak separation.

The uniaxial to uniaxial phase transition is one which has been studied most extensively using deuterium NMR. The quadrupole splittings of each phase can be easily evaluated from the peak separation in the composite spectrum. The H_α to Int phase transition in the NaTD–D_2O system was studied at 347 K using the line shape fitting method described here. The calculated phase boundaries obtained in this way are 52.8–55.2 wt % NaTD. This compares favorably with 52.8–56.3 wt % as shown in Figure 1B. The linear regression of two-phase samples to obtain tie-line end points for the four first-order phase transitions studied is summarized in Figure 12. In each of these transitions, the mole fraction of the individual liquid crystalline phases was obtained by optimizing the sum of the squared residuals in performing the line shape fitting as described above.

Comparison to Previous Work. The majority of studies relating to the lyotropic liquid crystalline phase behavior of surfactant–water mixtures have been of single-phase samples. The analysis of multiple-phase samples has been limited for several reasons. First, optical microscopy has been used to study a range of compositions in a single sample.[7,13-17] The single-phase regions have been identified, but the transitions have been largely ignored. Second, X-ray diffraction has also been applied to single-phase samples to characterize the unit cell and the repeat units which describe the phase structure.[3-10] Multiple-phase regions have been added to connect single-phase regions in a manner consistent with the Gibbs phase rule. Finally, NMR study of liquid crystal samples has identified multiple-phase regions as indicated by a composite spectrum.[10,15,16,24,28,30-37,40] These references only mention the use of line shape analysis to identify the

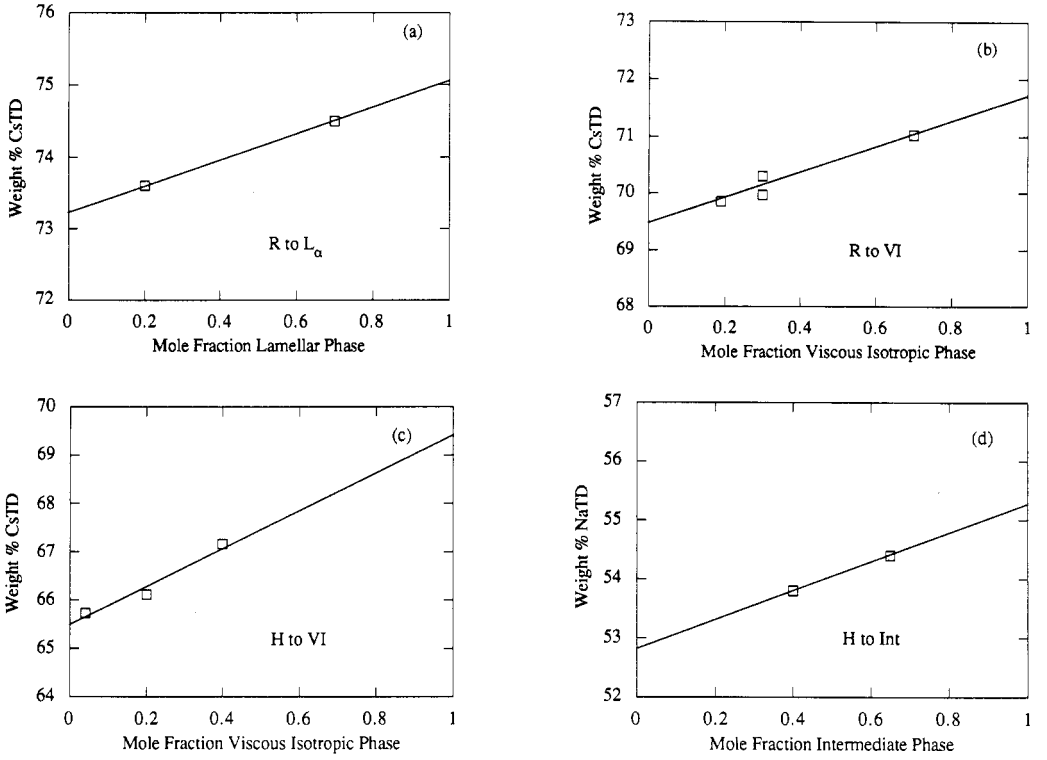

Figure 12. Calculated phase compositions for the first order-liquid crystalline phase transitions studied: (a) ribbon to lamellar phase transition (CsTD, 308 K), (b) ribbon to viscous isotropic phase transition (CsTD, 315 K), (c) hexagonal to viscous isotropic phase transition (CsTD, 335 K), and (d) hexagonal to intermediate phase transition (NaTD, 347 K).

existence of a multiple-phase region rather than the amounts of each phase.

One study used an approximate integration of the NMR spectra to determine the phase compositions of multiple-phase samples.[24] In those studies, it was noted that it was possible to extract phase compositions from the NMR data, but the calculations required to deconvolute the overlapping portion of the spectra were not performed. Moreover, theoretical spectra were not used to evaluate the relative amounts of each phase, and the integrals of each spectrum were not referenced to those of a single-phase spectrum. It was thus not possible to quantitatively determine tie line end points in these studies.

Conclusions

Deuterium NMR can be applied to surfactant–water liquid crystal systems and used for phase determination in a sample. The technique is especially powerful as it is noninvasive to the sample and can detect small (<10% of the sample) amounts of a phase in the sample. Two-phase liquid crystal samples, which are difficult to analyze using X-ray diffraction and polarizing microscopy, can be identified using deuterium NMR.

Theoretical line shapes were calculated to match experimental spectra using a least-squares minimization. The relative amounts of each phase in a sample were measured by the relative intensities of each characteristic spectrum. Using this information, the extent of two-phase regions was successfully quantified using a small number of biphasic samples. Phase transitions studied were ribbon phase to lamellar phase, ribbon phase to viscous isotropic phase, hexagonal phase to viscous isotropic phase, and hexagonal phase to intermediate phase. A variety of line shapes including uniaxial, biaxial, and isotropic were used to study the CsTD–D_2O and the NaTD–D_2O systems.

The primary strength of this technique is the quantitative determination of phase transition boundaries. In the R phase to L_α phase transition, the location of the lower concentration boundary is obscured by the overlap of the two spectral contributions. Being able to determine the limits of the biphasic region using samples away from the boundary is a useful ability.

Acknowledgment. This work was supported by NSF Grant CPE-8404599 and by discretionary grants from Colgate-Palmolive and the 3M Co.

Registry No. CsTD, 14912-90-4; NaTD, 822-12-8.